International Journal of General Medicine

Dovepress
Taylor & Francis Group

Open Access Full Text Article

ORIGINAL RESEARCH

RETRACTED ARTICLE: MCU-Mediated SIRT3 Inhibition Drives Oxidative Stress-Induced Cytoskeletal Disruption in Pancreatic Ductal Epithelium: A Mechanism of Hypertriglyceridemic Acute Pancreatitis

Junbo Hong[1], Qingzi Fu[2], Liang Zhu[1], Zhenzhen Yang[1], Jianhua Wan[1], Chaofeng Chen[1], Feng Chen[1], Shiyu Zhang[1]

[1]Department of Gastroenterology, Jiangxi Provincial Key Laboratory of Digestive Diseases, Jiangxi Clinical Research Center for Gastroenterology, Digestive Disease Hospital, The First Affiliated Hospital, Jiangxi Medical College, Nanchang University, Nanchang, Jiangxi, People's Republic of China; [2]Department of Medical Genetics, Jiangxi Maternal and Child Health Hospital, Nanchang, People's Republic of China

Correspondence: Shiyu Zhang, Email ndyfy09676@ncu.edu.cn

Purpose: The pathogenesis of hypertriglyceridemia -induced pancreatitis (HTGP) is complex and not fully understood. The purpose of this study was to investigate the molecular mechanism of the mitochondrial Ca uniporter (MCU) in HTGP.

Methods: We observed the expression levels of MCU and silent information regulator 3 (SIRT3) in both in vivo and in vitro HTGP models, and after intervention with ruthenium red (RR), an active inhibitor of MCU, and 3-(1H-1,2,3-triazol-4-yl) pyridine (3-TYP), an active inhibitor of SIRT3, changes in mitochondrial calcium ion, oxidative stress-related indices, the microfilament cytoskeleton, and monolayer cell permeability were detected.

Results: In vivo and in vitro experiments revealed the upregulation of MCU and downregulation of SIRT3 in caerulein-treated HPDE6-C7 cells and mice, along with increased mitochondrial calcium accumulation, increased reactive oxygen species (ROS) and malondialdehyde (MDA) levels, decreased glutamylcysteine (GSH) levels, destruction of the microfilament cytoskeleton, and increased monolayer permeability. During in vitro experiments, intervention with RR, an active inhibitor of MCU, reversed the above changes, whereas intervention with 3-TYP, an active inhibitor of SIRT3, further exacerbated the above changes.

Conclusion: MCU may be involved in the pathogenesis of AP by inhibiting the expression of SIRT3, resulting in increased oxidative stress and destruction of the microfilament cytoskeleton and pancreatic ductal mucosal barrier (PDMB) functions.

Keywords: pancreatitis, MCU, pathogenesis, oxidative stress, cytoskeleton

Introduction

Acute pancreatitis (AP) is a common problem in gastroenterology, with an annual incidence of up to 40 per 100,000 person-years in developed countries.[1] About 20% of all patients with AP have moderate-to-severe AP, for which the mortality rate is 20–40%.[2–4] Emerging evidence positions hypertriglyceridemia as a principal acute pancreatitis trigger, second only to biliary tract infections.[5] Owing to improvements in medical technology, the overall mortality rate of AP has decreased significantly,[6] but the mortality rate of severe AP is still about 28%.[7] Compared with other etiologies, hypertriglyceridemic acute pancreatitis (HTGP) is associated with accelerated disease progression, frequently leading to severe complications, including systemic inflammatory response syndrome (SIRS) and multiple organ dysfunction syndrome (MODS), which contribute to poor prognoses and high recurrence rates.[8] Therefore, the pathogenesis of AP, especially HTGP, needs to be elucidated, as it is poorly understood.

The toxicity of free fatty acids (FFAs) and the inflammatory response and release of large quantities of calcium ions caused by FFAs play key roles in the pathogenesis of HTGP.[9] High concentrations of FFAs are generated from TG hydrolysis by lipases in pancreatic tissues. They may trigger self-digestion of the pancreas by damaging pancreatic acinar

Received: 26 May 2025
Accepted: 21 August 2025
Published: 4 September 2025

cells and vascular endothelial cells, activating trypsinogen and protein kinase C, and releasing intracellular calcium.[10] In HTGP animal models, the accumulation of high levels of FFAs leads to ischemia, triggering acidosis and converting trypsinogen into active trypsin, leading to digestion of the pancreas.[11] However, existing research has focused predominantly on pancreatic acinar cells, whereas pancreatic ductal cells remain relatively understudied.

The concept of the pancreatic ductal mucosal barrier (PDMB) was first proposed in 1969.[12] This barrier, which is composed of a tightly packed layer of ductal epithelial cells and mucus, protects the pancreatic parenchyma from the contents of the pancreatic duct, such as bile and trypsin.[12] Actin filaments, key components of the cytoskeleton, are essential for providing mechanical support and maintaining cell morphology.[13] F-actin binding is necessary to promote the formation of adherens junctions (AJs) and tight junctions (TJs).[14] Endothelial barrier integrity and cell-cell junction stability are critically regulated by actin cytoskeletal dynamics.[15] Furthermore, FFAs induce actin reorganization and provoke pancreatic acinar cell impairment through elevated cytosolic Ca^{2+} concentrations, establishing a mechanistic link to HTGP pathogenesis.[16] Our previous studies revealed that the synthetic cholecystokinin analog caerulein (CAE) can induce AP in the human pancreatic duct epithelial cell line HPDE6-C7 and lead to increased permeability of monolayer cells;[17] however, the specific mechanism still needs further investigation.

The mitochondrial Ca^{2+} uniporter (MCU) is located in the inner mitochondrial membrane and functions mainly to transport calcium ions from the cytoplasm to the mitochondria. It plays a crucial role in the regulation of mitochondrial homeostasis, cell survival, and aerobic metabolism.[18] Under pathological conditions, calcium ion accumulation in mitochondria caused by the overexpression of MCU can impair mitochondrial function, increase the production of reactive oxygen species (ROS), decrease ATP synthesis, and even promote apoptosis.[19] Excessive uptake of mitochondrial calcium strongly influences the production of mitochondrial ROS.[19] Calcium ions may lead to an increase in ROS production by directly altering the performance of mitochondrial membranes.[20] In addition, the inhibition of MCU can significantly alleviate acute pancreatitis in mice; however, the specific mechanism is unclear.[21]

The active form of silent information regulator 3 (SIRT3) is located in mitochondria and functions in the deacetylation of target proteins. SIRT3 modulates mitochondrial protein expression and activation, reduces ROS generation, and is important for mitochondrial adaptability and the stress response.[22] Recent studies have shown that the activation of SIRT3 can effectively alleviate acute pancreatitis injuries,[23,24] suggesting that the inhibition of SIRT3 plays an important role in the pathogenesis of acute pancreatitis. However, whether MCU-mediated modulation of SIRT3 contributes to the pathogenesis of AP requires further investigation.

While numerous studies have shown calcium ion accumulation in mitochondria and cellular injury caused by ROS, the specific involvement of MCU-mediated mitochondrial calcium entry and ROS in pancreatic duct epithelial cells during HTGP has not yet been described. It also remains unclear whether MCU-associated mitochondrial calcium buildup influences the integrity of the pancreatic ductal epithelial mucosal barrier and the organization of the cytoskeleton in these cells. Therefore, in this study, we investigated the mechanism by which MCU and ROS affect the pancreatic ductal mucosal barrier in HTGP by inhibiting the activity of MCU and interfering with ROS production.

Methods

Formation of Experimental Groups

To conduct in vitro studies, HPDE6-C7 human pancreatic duct epithelial cells (Shanghai Jingfeng Biotechnology Co., Ltd., GT1730C) were treated with CAE (100 nM/L, Amquar, EYS113, USA), triglycerides (TG, 2.5 mM/L, Solarbio, T9420, China), ruthenium red (RR, 10 mM/L, Amquar, EI2414, USA) and 3-(1H-1,2,3-triazol-4-yl) pyridine (TYP, 0.25 μmol/L, Amquar, EI2418, USA) for 24 h and then divided into twelve groups: the control group, TG group, CAE group, TG+CAE group, RR group, TG+RR group, CAE+RR group, TG+CAE+RR group, TYP group, TG+TYP group, CAE+TYP group, and TG+CAE+TYP group. In vivo, 20 mice were randomly divided into the following four groups: the control group, HTG group, AP group, and HTGP group. All the experiments in this study were conducted between June 2023 and December 2024.

Animals

The study was approved by the Ethics Committee of the First Affiliated Hospital of Nanchang University (CDYFY-IACUC-202311QR029 and CDYFY-IACUC-202409GR018). All experimental procedures were performed in strict compliance with the National Standards for Laboratory Animal Welfare in China (GB/T 35892–2018), ARRIVE Guidelines 2.0, and the 3Rs principles (Replacement, Reduction, Refinement). Four-week-old wild-type male C57BL6/J mice were purchased from Changsha Tianqin Biotechnology Co., Ltd. All the mice were housed at 22–24 °C in a specific pathogen-free environment and were provided free access to food and water for four weeks. The mice in the control group and acute AP group were fed an ordinary diet (11001, Boaigang. China), and the mice in the HTG group and HTGP group were fed a high-fat diet (1160HLP, Boaigang, China). After the mice were fed for four weeks, they were intraperitoneally injected with 50 μg/kg CAE (EYS113, Amquar, USA) seven times at 1 h intervals to induce AP. The mice in the control group and HTG group were intraperitoneally injected with the same volume of normal saline. Blood was collected from the inferior vena cava of each mouse to determine amylase and triglyceride levels 24 h after the last intraperitoneal injection. Pancreatic tissue was removed for H&E staining, immunohistochemistry, and WB analysis.

Cell Culture

The HPDE6-C7 human pancreatic duct epithelial cell line was obtained from Guangzhou Jennio Biotechnology Co., Ltd., China. Cells were maintained under sterile conditions at 37 °C in an atmosphere containing 5% CO_2. The complete culture medium (100 mL) consisted of 89 mL MEM (8120294, Gibco, USA), 10 mL FBS (A511-001, Lonsera, Uruguay), and 1 mL penicillin/streptomycin (P1400, Solarbio, China). Cells were seeded into sterile Petri dishes (60 mm diameter; 430166, Corning, USA) at a density of 1 × 10⁶/mL. Upon reaching approximately 70% confluence, cultures from different groups were exposed to varying concentrations of the designated intervention agents for a duration of 24 h.

H&E Staining

Pancreatic tissues were immersed in 4% paraformaldehyde solution for 12 h, embedded in paraffin, and cut into thin sections. Three random fields in each section were selected to calculate the pancreatic histopathological score. The pancreatic histopathological scoring was performed following the criteria described by Van Laethem et al.[25]

Immunohistochemistry

Dewaxing, hydration, and thermal repair were performed, and then, 5 μg/mL primary antibody (A00685-1, Boster, China) was added and incubated overnight at 4 °C. After the tissues were incubated with an HRP-labeled linked polymer (KIT-5009, MXB biotechnologies, China) for 40 min at 26 °C, the signal was detected using DAB (P0202, Beyotime, China). Three randomly selected fields of view per sample were captured under an inverted microscope (CKX41, Olympus, Japan) and analyzed using ImageJ software (version 1.53t) to calculate the average optical density (AOD) values.

Serum Triglyceride and Amylase Detection

Mouse venous blood was stored at 26 °C for 2 h and centrifuged at 4 °C at 3000 RPM for 15 min, after which the supernatant was collected for analysis. All steps in the procedure were performed in strict accordance with the instructions of the triglyceride detection kit (c061-a, Changchun Huili, China) and the amylase detection kit (C033, Changchun Huili, China). The levels of triglycerides and amylase were calculated on the basis of the absorbance measured via a microplate reader (Varioskan LUX, Thermo, USA).

Protein Extraction

After the medium was removed, the cells were washed three times with PBS (P1020, Solarbio, China). Next, 1000 μL of RIPA lysis solution (P0013K, Beyotime, China) containing 10 μL of phenyl methane sulfonyl fluoride (P0100, Solarbio, China) was added to each 60 mm Petri dish, and the cells were placed on ice for 30 min before centrifugation (4 °C at

12000 RPM for 15 min). Then, 200 μL of the supernatant was collected, 50 μL of protein loading buffer (P1015, Solarbio, China) was added, and the mixture was mixed. Next, the mixture was heated at 100 °C for 10 min to denature the protein. The total protein was stored in a refrigerator at –20 °C.

Western Blotting Analysis

Proteins were resolved by SDS-PAGE and then transferred to a 0.22 μm PVDF membrane. The membrane was blocked with a 5% skim milk powder solution at 26 °C for 45 min. After three washes with TBST solution, the membrane and primary antibodies (D2Z3B, CST, UK, 1:1000) were incubated at 4 °C for 12 h. After washing again with TBST, the membrane and secondary antibodies (5151P, CST, UK, 1:10000) were incubated at 26 °C in the dark for 1 h. The fluorescence signal was detected using a Li-COR Odyssey dual-color infrared fluorescence imaging system.

Cytotoxicity Assay

A Cell Counting Kit-8 (CCK-8, C0038) was purchased from Beyotime Biotechnology Co., Ltd. HPDE6-C7 cells were seeded in 96-well plates at a density of 5000 cells/100 μL. Five different final concentrations of ruthenium red (1 μmol/L, 5 μmol/L, 10 μmol/L, 50 μmol/L, and 100 μmol/L) were used. After incubation for 24 h in 5% CO_2 at 37 °C, 10 μL of CCK-8 solution was added to each well and incubated in the cell culture box for another 1 h. Finally, the absorbance was measured at 450 nm.

Mitochondrial Calcium Ion Detection

DMSO (D8371, Solarbio, China) was added to 50 μg of Rhod-2 AM (R1245MP, Invitrogen, USA) to produce 100 μL of mother liquor at a concentration of 4 mmol/L, which was stored at –20 °C. Next, 6 μL of mother liquor was added to 5994 μL of HBSS (H1025, Solarbio, China) to prepare a working solution with a concentration of 4 mmol/L. After the medium was removed and the cells were washed three times with HBSS, 1 mL of stock solution was added to each 60 mm petri dish and incubated at 37 °C for 30 min. After washing once with PBS, 1 mL of HBSS was added, and the mixture was incubated at 37 °C for 30 min. After washing with PBS twice, 1 mL of mitochondrial green fluorescent probe (Mito-Tracker Green, C1048, Beyotime, China) diluted 5000 times with HBSS was added, and the mixture was incubated at 37 °C for 15 min. The red and green fluorescence signals were imaged under an inverted fluorescence microscope (CKX41, Olympus, Japan) after the samples were washed twice with PBS. After three fields of view were randomly selected for each sample, ImageJ software was used to calculate the mean fluorescence intensity value for subsequent statistical analysis.

ROS Detection

When the degree of HPDE6-C7 cell fusion in a 60 mm diameter sterile Petri dish reached 70%, the cells were washed with PBS three times, and then 2 mL of serum-free medium supplemented with 10 mM/L DCFH-DA (S0033S, Beyotime, China) was added to each dish. The cells were incubated for 20 min in a cell culture box at 37 °C and washed with serum-free cell culture medium three times. Then, the green fluorescence images captured under a fluorescence microscope (CKX41, Olympus, Japan) were analyzed via ImageJ software. Similarly, we randomly selected three regions to calculate the average fluorescence intensity for subsequent statistical analysis.

Malondialdehyde (MDA) Detection

The cells in the six-well plate were lysed with RIPA lysis buffer (P0013K, Beyotime, China) for 30 min and then centrifuged. The supernatant was collected for subsequent analysis.

An MDA detection kit (S0131S, Beyotime, China) was obtained from Biotime Biotechnology Co., Ltd. The MDA working solution and standard were prepared in accordance with the manufacturer's protocol. A total of 100 μL of standard solutions at varying concentrations, along with samples from different groups, was mixed with 200 μL of the MDA working solution and incubated in boiling water for 15 min. Following cooling to 26 °C, the mixtures were centrifuged at 1000 ×g for 10 min at 26 °C. Subsequently, 200 μL of the supernatant was transferred to a 96-well plate,

and absorbance was measured at 532 nm using a microplate reader. MDA concentrations were determined based on the corresponding standard curve.

A BCA protein concentration determination kit (P0010, Beyotime, China) was purchased from Biotime Biotechnology Co., Ltd. The BCA working solution and protein standard were prepared following the manufacturer's instructions. In each well of the 96-well plate, 20 μL of protein standard or test sample at different concentrations was added successively, followed by the addition of 200 μL of BCA working solution. After the plate was incubated for 30 min at 37 °C, the absorbance was measured at 562 nm using a microplate reader. The protein concentration of each group was calculated based on a standard curve. The amount of MDA per milligram of protein was calculated by dividing the concentration of MDA by the corresponding total protein concentration.

Gamma-Glutamylcysteine (GSH) Detection

After HPDE6-C7 cells were washed with PBS three times, the cells were resuspended and lysed by ultrasonication. The broken cell suspension was centrifuged at 3500 rpm for 10 min, after which 0.1 mL of the supernatant was removed for subsequent analysis. Following the instructions of the GSH and GSSH determination kits (S0053, Beyotime, China), 0.1 mL of reagent 1, 0.1 mL of reagent 2, and 0.025 mL of reagent 3 were added to the wells containing the blank, standard, and test samples, respectively. The plate was left undisturbed for 5 min, after which the absorbance was measured at 405 nm using a microplate reader.

Immunofluorescence Microfilament Staining

After HPDE6-C7 cells were washed on sterile glass plates twice with PBS at 37 °C, 4% paraformaldehyde was added at 26 °C for 10 min. The cells were again washed twice with PBS, and then 0.5% Triton X-100 was added for 5 min. Next, 200 μL of phalloidin (200 nmol/L; CA1610, Solarbio, China) was added to the glass plate and incubated at 37 °C in the dark for 30 min. After washing twice with PBS, 200 μL of DAPI (100 nmol/L; S2110, Solarbio, China) was added to stain the nuclei. Finally, the morphological characteristics of the microfilaments were observed under a fluorescence microscope (CKX41, Olympus, Japan).

Permeability Test of Monolayer Cells

First, 100 μL of complete medium containing about 100,000 cells was added to the apical compartment of the Transwell system (3413, Corning, USA), and 600 μL of complete medium was added to the basolateral compartment. After 24 h of culture in an incubator at 37 °C, the different groups were treated with the corresponding intervention agent for 24 h. After the culture medium was removed and the cells were washed with PBS three times, 200 μL of FITC-Dextran 4000 (1 mg/mL, 46944, Sigma, USA) was added to the apical compartment, and 600 μL of PBS was added to the basolateral compartment. The cells were then incubated for 2 h. After incubation, 2 μL of liquid from the basolateral compartment was removed from the 96-well plate, and the absorbance was measured via a microplate reader (excitation/emission wavelength: 490/520 nm).

Statistical Methods

The measurement data were statistically analyzed via the unpaired sample *t*-test in GraphPad Prism 8 software, and $P<0.05$ was considered statistically significant.

Results

An acute pancreatitis model in mice and HPDE6-C7 cells was established successfully. The expression of MCU in the pancreatic tissue of the mice in the AP group and HTGP group was significantly greater than that in the control group, and the increase in the HTGP group was significantly higher compared to the AP group. The expression of SIRT3 in the pancreatic tissue of the mice in the AP group and HTGP group was significantly lower than that in the control group, and the decreasing trend in the HTGP group was more obvious than that in the AP group.

H&E staining revealed prominent tissue edema, significant widening of the interlobular space, and infiltration of many inflammatory cells in the pancreatic tissues of the mice in the AP and HTGP groups (Figure 1A–D). The pancreatic

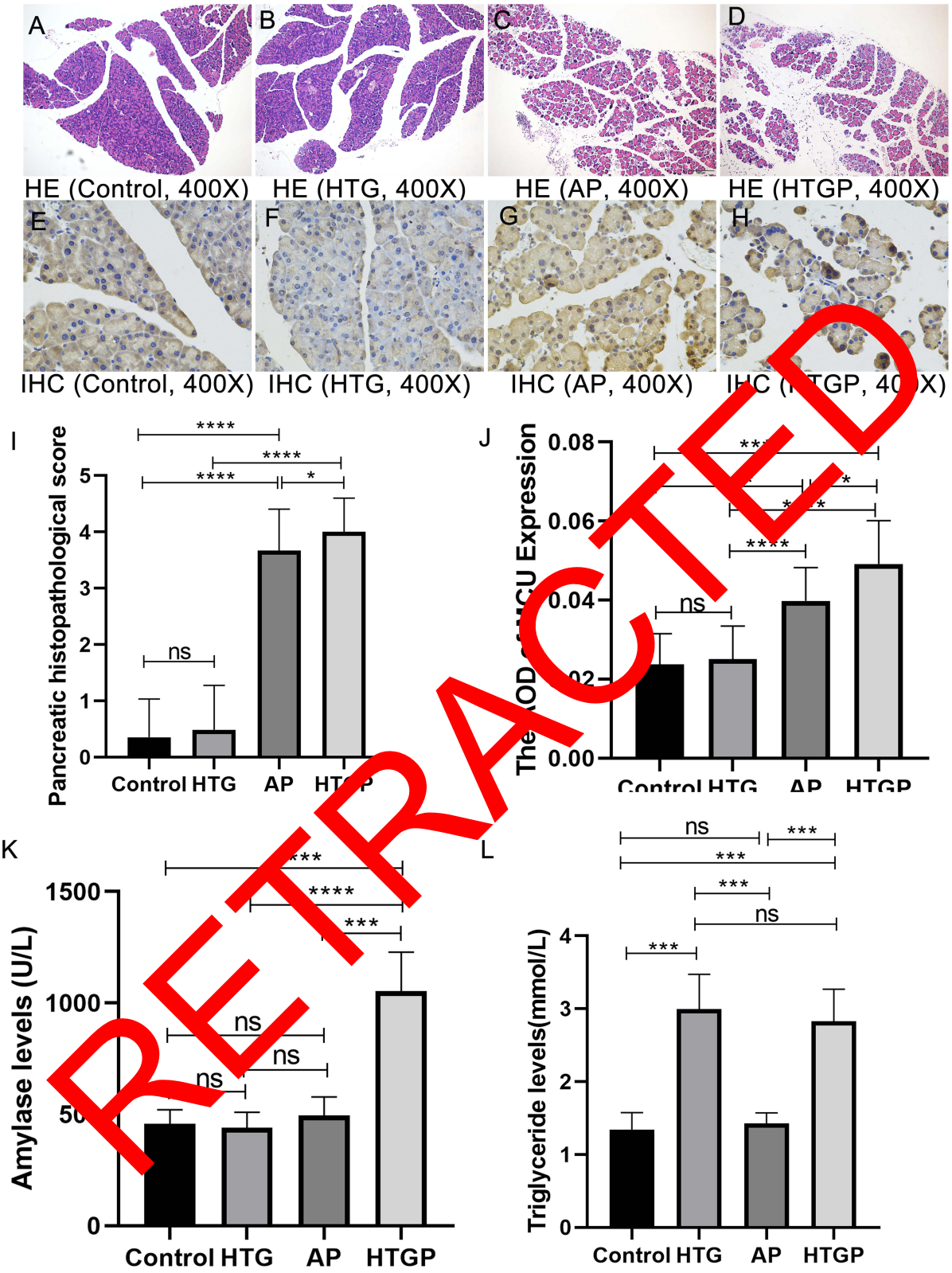

Figure 1 Mouse models of AP, HTG and HTGP were successfully constructed. (**A**–**D**) HE staining of pancreatic tissue from the mice in each group. (**E**–**H**) Immunohistochemical staining images of MCU in the pancreatic tissue of the mice in each group. The brown region in the figure is the MCU-positive region, and the darker the brown region is, the greater the expression of MCU. (**I**) Pancreatic histopathological scores of the mice in each group. (**J**) AOD values of the MCU immunohistochemistry results of the mice in each group. (**K**) Blood amylase levels in each group of mice; (**L**) Serum triglyceride levels of the mice in each group. **P* < 0.05; ***P* < 0.01; ****P* < 0.001; *****P* < 0.0001.

Abbreviations: AP, acute pancreatitis; HTGP, hypertriglyceridema-induced pancreatitis; AOD, average optical density.

histopathological scores of the AP group and HTGP group were significantly greater than those of the control group and HTG group, respectively (Figure 1I; AP vs control, t = 22.13, P < 0.0001; HTG vs HTGP, t = 24.65, P < 0.0001). No significant difference was recorded in the serum amylase levels between the AP group and the control group (Figure 1K, AP vs control, t = 0.81, P = 0.44), but the serum amylase level in the HTGP group was significantly greater than that in the HTG group and AP group (Figure 1K, HTG vs HTGP, t = 24.65, P < 0.0001; AP vs HTGP, t = 6.21, P < 0.001). The serum triglyceride levels in the HTG and HTGP groups were significantly greater than those in the control and AP groups (Figure 1L, HTG vs control, t = 7.01, P < 0.001; HTGP vs AP, t = 6.56, P < 0.001).

Immunohistochemical analysis showed that the AOD of MCU in the AP and HTGP groups was significantly higher than that in the control and HTG groups (Figure 1E–H, and J; AP vs control, t = 5.27, P < 0.0001; HTG vs HTGP, t = 6.84, P < 0.0001). Western blot results were consistent with these findings, indicating that MCU expression in the AP group was significantly elevated compared to the control group (Figure 2A and B; AP vs control, t = 7.63, P < 0.05). MCU expression in the HTGP group was also significantly higher than in both the HTG and AP groups (Figure 2A and B; HTGP vs HTG, t = 7.99, P < 0.01; HTGP vs AP, t = 5.76, P < 0.01). Likewise, in vitro experiments demonstrated that MCU expression in the CAE group was significantly greater than in the control group (Figure 2C and D; CAE vs control, t = 9.11, P < 0.001), and the TG+CAE group exhibited significantly higher MCU levels than both the TG and CAE groups (Figure 2C and D; TG+CAE vs TG, t = 6.71, P < 0.01; TG+CAE vs CAE, t = 4.89, P < 0.05).

The expression level of SIRT3 in the AP and HTGP groups was significantly lower than that in the control and HTG groups (Figure 2E; AP vs control, t = 3.841, P < 0.05; HTGP vs HTG, t = 15.74, P < 0.0001). The expression level of SIRT3 in the HTGP group was also significantly lower than that in the AP group (Figure 2E; HTGP vs AP, t = 6.105, P < 0.01). The same results were observed via immunohistochemistry (Figure 2F and G; AP vs control, t = 8.067, P < 0.0001; HTGP vs HTG, t = 9.816, P < 0.0001).

In vitro experiments demonstrated that SIRT3 expression was downregulated in both the CAE and TG+CAE groups, accompanied by a significant increase in the mitochondrial calcium ion concentration and increased oxidative stress (evidenced by elevated ROS and MDA levels, as well as decreased GSH levels). Additionally, microfilament cytoskeleton disruption and increased monolayer cell permeability were observed. Notably, RR intervention significantly reversed these changes.

Ruthenium red at a concentration of ≤10 μM maintained cell viability at about 90%, whereas ruthenium red at a concentration of >10 μM significantly inhibited cell viability (Figure 3C). Therefore, in subsequent in vitro experiments, we used ruthenium red at a concentration of 10 μM. 3-TYP at a concentration of ≤0.25 μM maintained cell viability at about 90%, whereas 3-TYP at a concentration of >0.25 μM significantly inhibited cell viability (Figure 3D and E). Therefore, in subsequent in vitro experiments, we used 3-TYP at a concentration of 0.25 μM.

The expression level of SIRT3 in the CAE and TG+CAE groups was significantly lower than that in the control and TG groups (Figure 3A and B; CAE vs control, t = 9.903, P < 0.001; TG+CAE vs TG, t = 8.730, P < 0.001). The expression level of SIRT3 in the TG+CAE group was also significantly lower than that in the AP group (Figure 3A and B; HTGP vs AP, t = 6.765, P < 0.01). There was no significant difference in the expression of SIRT3 between the RR and control groups or between the TG+RR and TG groups (Figure 3A and B; RR vs control, t = 1.531, P > 0.05; TG+RR vs TG, t = 1.857, P > 0.05).

The mean fluorescence intensity of mitochondrial calcium in the CAE group was markedly higher than in the control group (Figure 4A and B; CAE vs control, t = 15.49, P < 0.0001). In addition, the TG+CAE group exhibited significantly greater mitochondrial calcium fluorescence intensity compared with both the TG and CAE groups (Figure 4A and B; TG +CAE vs TG, t = 15.64, P < 0.0001; TG+CAE vs CAE, t = 3.47, P < 0.01). Treatment with ruthenium red notably reduced the elevated mitochondrial calcium levels observed in the CAE and TG+CAE groups (Figure 4A and B; CAE +RR vs CAE, t = 9.87, P < 0.0001; TG+CAE+RR vs TG+RR, t = 12.03, P < 0.0001).

The mean green fluorescence intensity of the ROS in the CAE and TG+CAE groups was significantly greater than that in the control and TG groups (Figure 4C and D; CAE vs control, 66.49 ±3.88 vs 41.82 ±2.52, t = 13.06, P < 0.0001; TG+CAE vs TG, 74.33 ±6.22 vs 37.79 ±5.37, t = 10.89, P < 0.0001), and this change was reversed by RR intervention (Figure 4C and D; CAE+RR vs CAE, 44.62 ±8.23 vs 66.49 ±3.88, t = 5.86, P < 0.001; TG+CAE+RR vs TG+CAE, 49.69 ±4.73 vs 74.33 ±6.22, t = 7.73, P < 0.0001). The MDA concentrations in the CAE and TG+CAE groups were

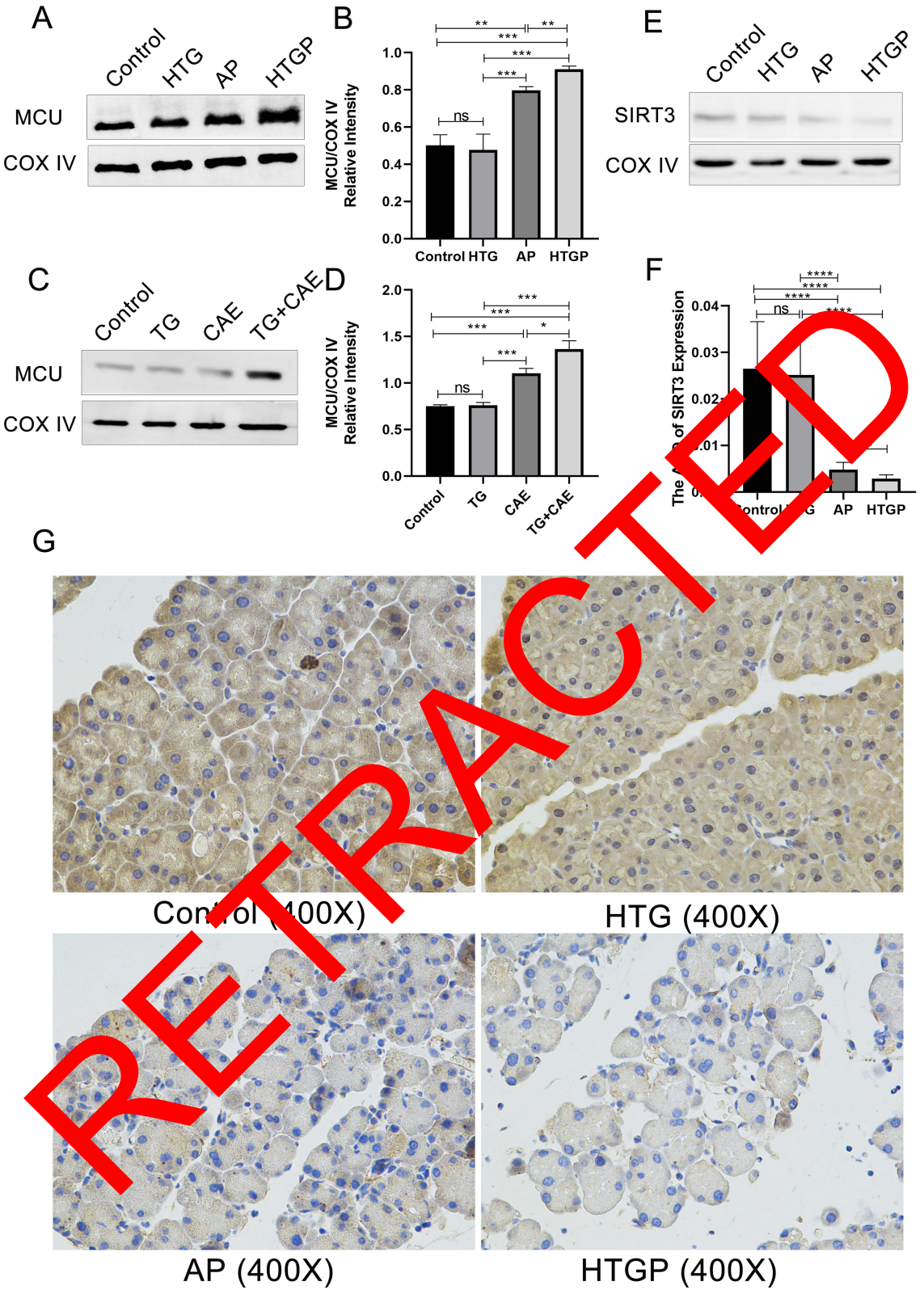

Figure 2 (**A**) Expression of MCU in the pancreatic tissues of each group of mice; COX IV was used as a loading control for Western blotting. (**B**) Relative expression level of MCU in the pancreatic tissues of each group of mice. The above results were obtained from three independent experiments. (**C**) Expression of MCU in HPDE6-C7 cells in each group. COX IV was used as a loading control for Western blotting. (**D**) Relative expression level of MCU in HPDE6-C7 cells in each group. The above results were obtained from three independent experiments. (**E**) Expression of SIRT3 in the pancreatic tissues of each group of mice. COX IV was used as a loading control for Western blotting. (**F**) AOD level of SIRT3 expression in the pancreatic tissues of each group of mice. (**G**) Immunohistochemistry analysis of SIRT3 expression in the pancreatic tissues of each group of mice. **P* < 0.05; ***P* < 0.01; ****P* < 0.001; *****P* < 0.0001.

Abbreviations: AP, acute pancreatitis; HTGP, hypertriglyceridemia-induced pancreatitis; AOD, average optical density.

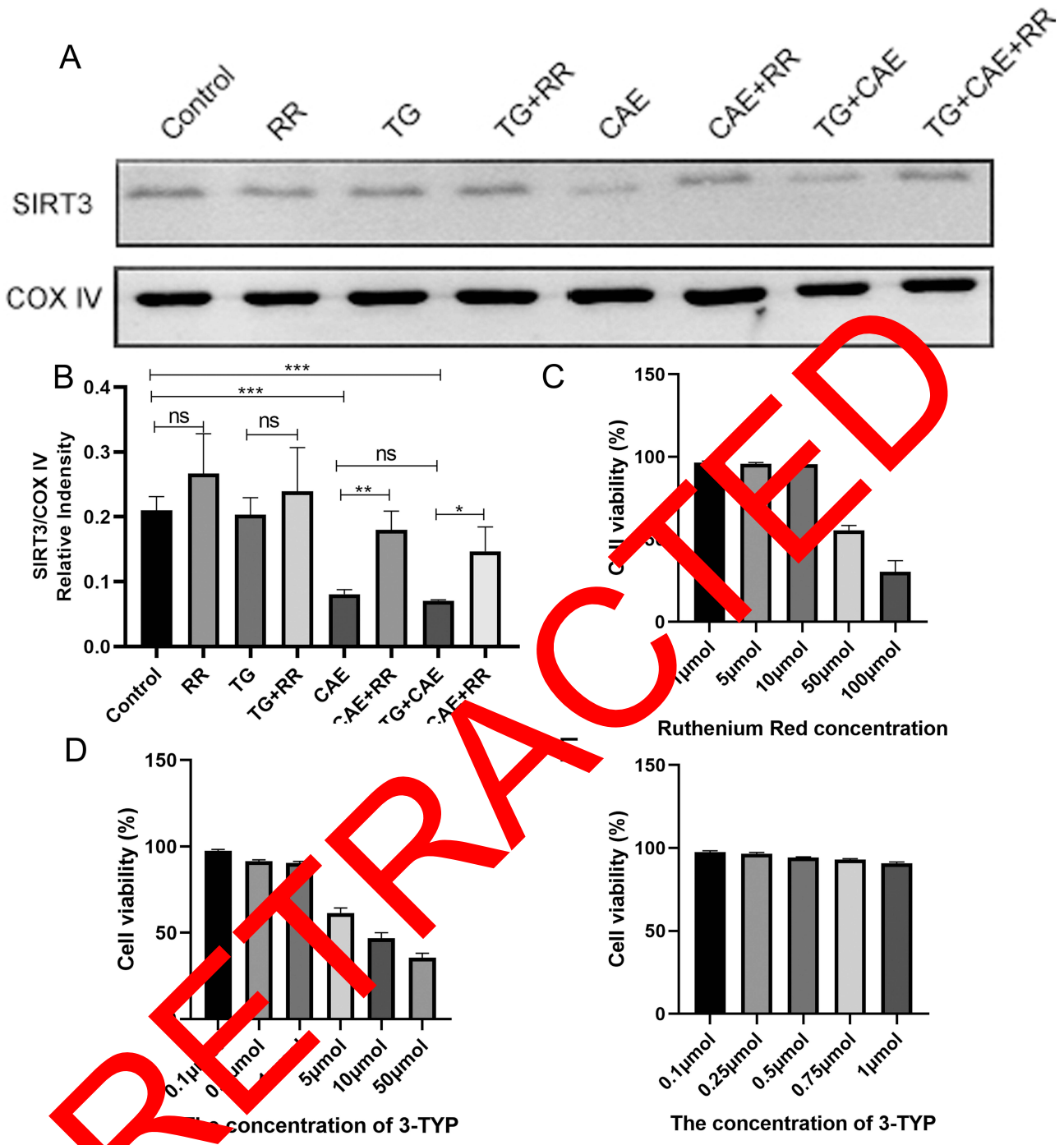

Figure 3 (**A**) Expression of SIRT3 in HPDE6-C7 cells in each group; COX IV was used as a loading control for Western blotting. (**B**) Relative expression level of SIRT3 in HPDE6-C7 cells in each group. The above results were obtained from three independent experiments. (**C**) Cytotoxicity assay of HPDE6-C7 cells cultured with different concentrations of ruthenium red. (**D** and **E**) Cytotoxicity assay of HPDE6-C7 cells cultured with 3-TYP at different concentrations; **P* < 0.05; ***P* < 0.01; ****P* < 0.001; *****P* < 0.0001.

significantly greater than those in the control and TG groups (CAE vs control, 0.236 ±0.008 vs 0.117 ±0.006, t = 20.04, P < 0.0001; TG+CAE vs TG, 0.267 ±0.011 vs 0.123 ±0.006, t = 20.46, P < 0.0001) (Figure 5A), and the MDA concentration increased more significantly in the TG+CAE group than in the CAE group (TG+CAE vs CAE, 0.267 ±0.011 vs 0.236 ±0.008, t = 4.063, P < 0.05). Ruthenium red intervention significantly decreased the increase in the MDA concentration in the CAE and TG+CAE groups (Figure 5A, TG+CAE+RR vs TG+CAE, 0.152 ±0.007 vs 0.267 ±0.011, t = 15.59, P < 0.0001; CAE+RR vs CAE, 0.14 ±0.014 vs 0.236 ±0.008, t = 9.886, P < 0.001). Compared with

https://doi.org/10.2147/IJGM.S542782

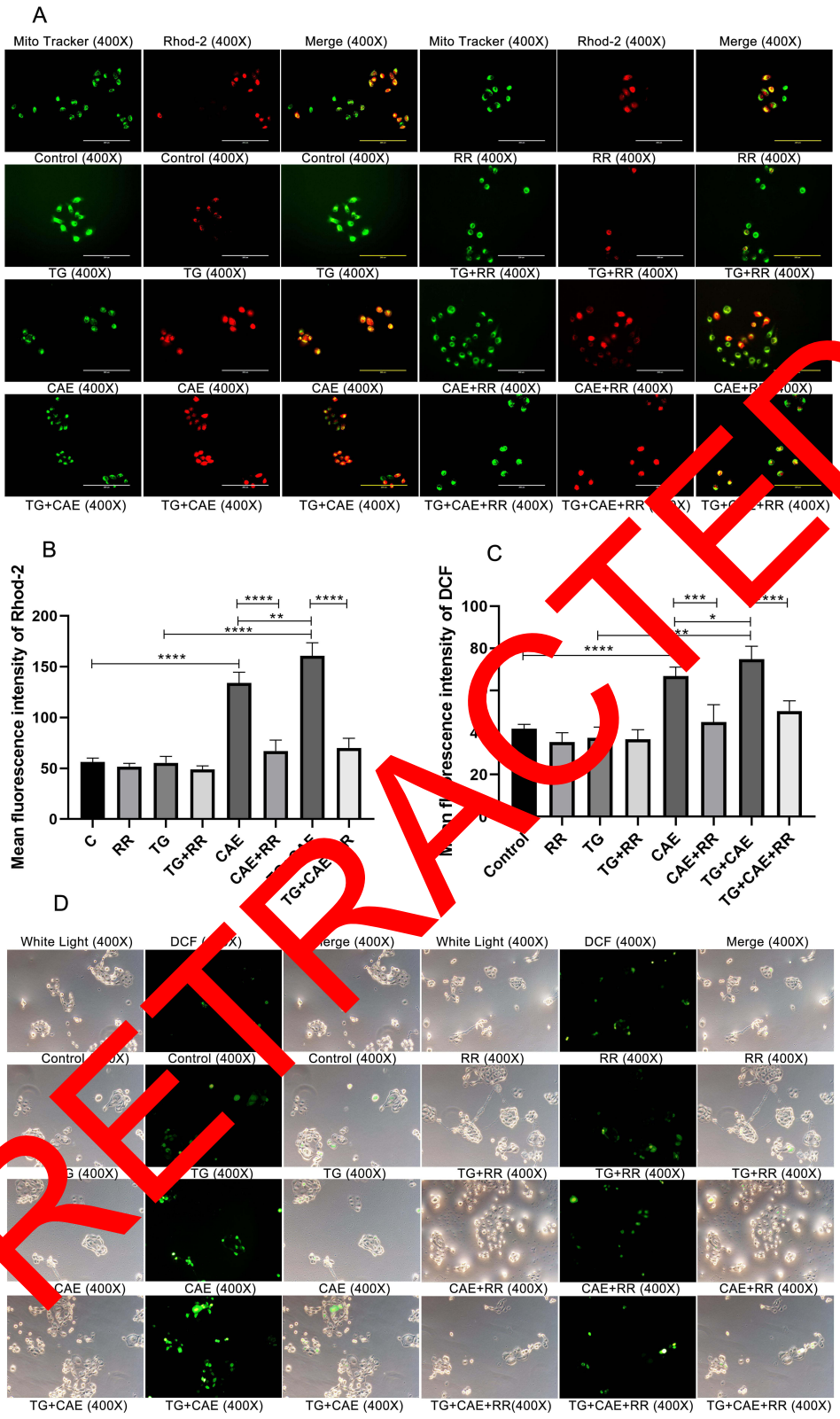

Figure 4 (**A**) Immunofluorescence images of mitochondrial calcium ions in HPDE6-C7 cells from each group. The stronger the red fluorescence is, the higher the concentration of mitochondrial calcium ions. (**B**) The average fluorescence intensity of the mitochondrial calcium ions in HPDE6-C7 cells in each group. (**C**) The average fluorescence intensity of the ROS in HPDE6-C7 cells in each group. (**D**), Immunofluorescence images of the ROS in HPDE6-C7 cells in each group; the stronger the green fluorescence is, the higher the concentration of ROS; **P* < 0.05; ***P* < 0.01; ****P* < 0.001; *****P* < 0.0001.

Abbreviation: ROS, reactive oxygen species.

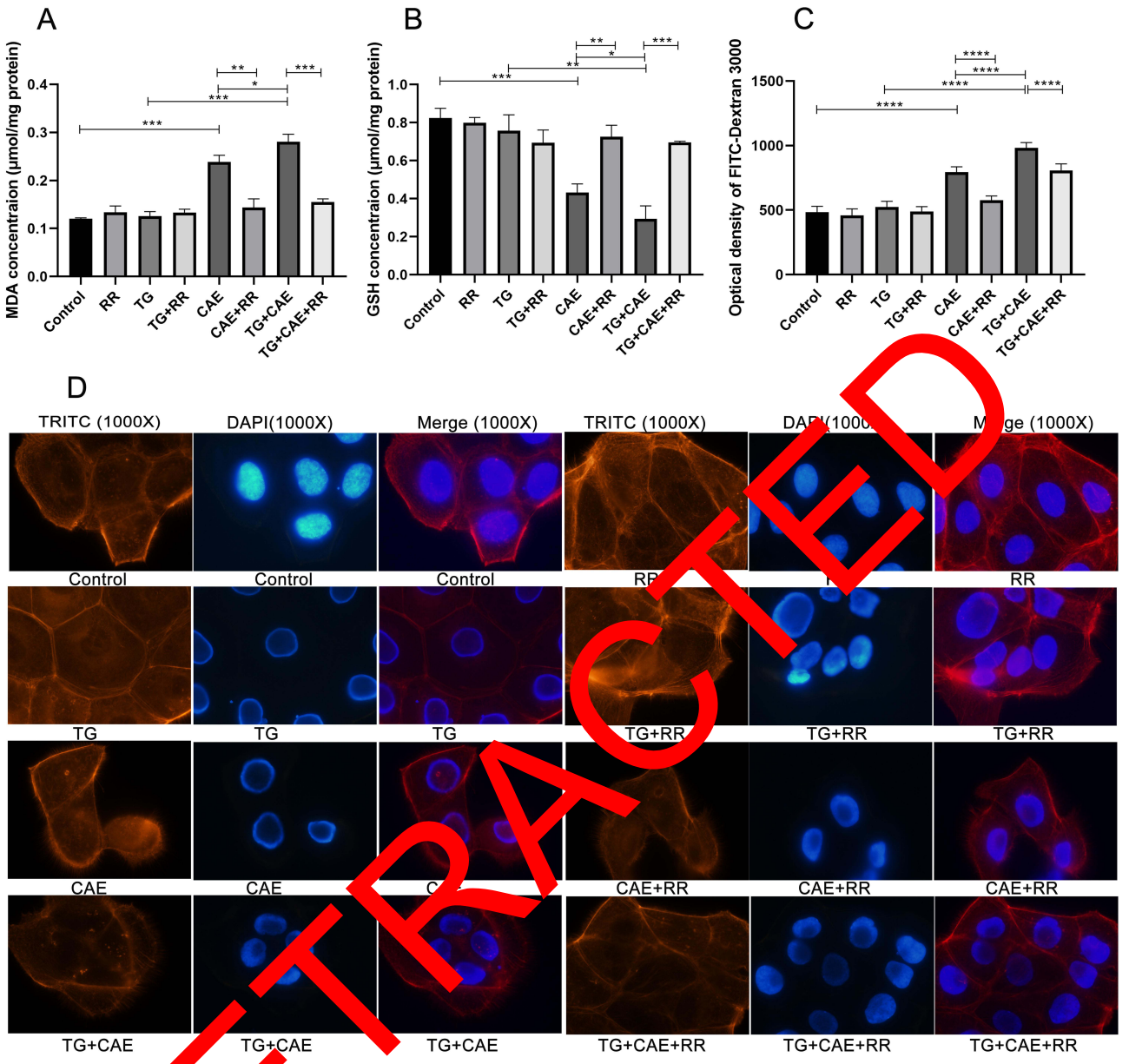

Figure 5 (**A**) Comparison of the MDA concentrations in HPDE6-C7 cells in each group. (**B**), Comparison of the GSH concentrations in HPDE6-C7 cells in each group. (**C**) Monolayer cell permeability of HPDE6-C7 cells in each group. (**D**) Microfilament cytoskeleton staining of HPDE6-C7 cells in each group, in which red indicates the microfilament cytoskeleton and blue indicates the nucleus. *$P < 0.05$; **$P < 0.01$; ***$P < 0.001$; ****$P < 0.0001$.

those in the control and TG+CAE groups, the GSH concentrations in the CAE and TG+CAE groups presented the opposite trend in terms of the MDA concentration (Figure 5B, CAE vs control, 0.435 ±0.041 vs 0.817 ±0.04, t = 11.51, P < 0.001; TG+CAE vs TG, 0.29 ±0.067 vs 0.751 ±0.074, t = 8.01, P < 0.01); however, this trend was weakened by RR intervention (Figure 5B, TG+CAE+RR vs TG+CAE, 0.689 ±0.018 vs 0.29 ±0.067, t = 9.926, P < 0.001; CAE+RR vs CAE, 0.722 ±0.055 vs 0.435 ±0.041, t = 7.266, P < 0.01).

In the control and TG groups, the microfilaments were regularly arranged in bundles. In the CAE and TG+CAE groups, the structural arrangement of the microfilaments was disordered, the bundle arrangement structure disappeared, and the microfilaments were loose and dispersed. After 24 h of RR intervention, the disordered arrangement, release, and dispersion of the microfilament structures in the CAE and TG+CAE groups were partially improved (Figure 5D).

The permeability of monolayer cells in the CAE and TG+CAE groups was significantly greater than that in the control and TG groups (Figure 5C, CAE vs control, 914.7 ±114.4 vs 585 ±178.9, t = 3.287, P < 0.05; TG+CAE vs TG,

https://doi.org/10.2147/IJGM.S542782

1239 ±142.3 vs 700.01 ±149.5, t = 3.367, P < 0.05). Additionally, the permeability of monolayer cells increased more significantly in the TG+CAE group than in the CAE group (Figure 5C, TG+CAE vs CAE, 1239 ±142.3 vs 914.7 ±114.4, t = 3.079, P < 0.05). Ruthenium red intervention significantly decreased the increase in monolayer cell permeability in the CAE and TG+CAE groups (Figure 5C, TG+CAE+RR vs TG+CAE, 786.3 ±237.6 vs 1239 ±142.3, t = 2.833, P < 0.05; CAE+RR vs CAE, 617.2 ±179 vs 914.7 ±114.4, t = 4.085, P < 0.05).

In vitro experiments revealed that intervention with 3-TYP, a specific inhibitor of SIRT3 activity, significantly exacerbated mitochondrial calcium ion accumulation, enhanced oxidative stress, disrupted the microfilament cytoskeleton, and increased monolayer cell permeability in both the AP and HTGP groups.

Intervention with 3-TYP significantly increased the accumulation of mitochondrial calcium ions in the CEA and TG+CAE groups (Figure 6A and B; CAE+TYP vs CAE, T = 8.86, P < 0.0001; TG+CAE+TYP vs TG+RR, t = 11.02, P < 0.0001).

Intervention with 3-TYP significantly increased ROS accumulation (Figure 6C and D, TG+CAE+TYP vs TG+CAE, 0.389 ±0.012 vs 0.267 ±0.011, t = 12.3, P < 0.001; CAE+TYP vs CAE, 0.338 ±0.028 vs 0.236 ±0.008, t = 6.098, P < 0.01) and the MDA concentration (Figure 7A, TG+CAE+TYP vs TG+CAE, 0.389 ±0.012 vs 0.267 ±0.011, t = 12.3, P < 0.001; CAE+TYP vs CAE, 0.338 ±0.028 vs 0.236 ±0.008, t = 6.098, P < 0.01) in the CAE and TG+CAE groups but decreased the GSH concentration in the CAE and TG+CAE groups (Figure 7B, TG+CAE+TYP vs TG+CAE, 0.151 ±0.016 vs 0.29 ±0.067, t = 3.509, P < 0.05, CAE+TYP vs CAE, 0.244±0.022 vs 0.[illegible]±0.041, t = 7.066, P < 0.01).

After 24 h of 3-TYP intervention, the disordered arrangement, release, and dispersion of the microfilament structures in the CAE and TG+CAE groups worsened (Figure 7D).

3-TYP intervention significantly increased monolayer cell permeability in the CAE and TG+CAE groups (Figure 7C, TG+CAE+TYP vs TG+CAE, 1443 ±107.2 vs 1206 ±87.45, t = 2.972, P < 0.05; CAE+TYP vs CAE, 1140 ±74.79 vs 981.3 ±52.98, t = 2.992, P < 0.05).

Discussion

Caerulein, a cholecystokinin analog, is widely used to induce AP in vivo[26] and in vitro.[27–29] In the present study, H&E staining revealed obvious tissue edema, significant widening of the interlobular space, and infiltration of many inflammatory cells in the pancreatic tissues of the mice in the AP and HTGP groups, indicating that the CAE-induced AP model mice successfully developed. In animal studies, the level of MCU expression in the AP group was significantly greater than that in the control group. In an in vitro study, the level of MCU expression in the CAE and TG+CAE groups was significantly greater than that in the control and TG groups, which was consistent with the results of the in vivo study. Moreover, significant changes in mitochondrial calcium ions, ROS, MDA, GSH, microfilament morphology, and monocyte permeability were also observed in the CAE and TG+CAE groups compared with those in the control group after 24 h of co-culture with HPDE6-C7 cells. Therefore, we hypothesized that the co-culture of CAE with HPDE6-C7 may constitute a new model of in vitro AP, which was also reported in our previous studies.[30,31]

In this study, the serum triglyceride levels were significantly greater in the hypertriglyceridemia group than in the non-hypertriglyceridemia group. Metabolites of triglycerides, ie, FFAs, are toxic to pancreatic tissue[32] and play important roles in the development of AP.[33] Unsaturated fatty acids can not only lead to hypocalcemia associated with a poorer prognosis by binding to calcium ions[34] but also increase the levels of tumor necrosis factor, interleukin-6, and other cytokines, triggering or aggravating AP.[35,36] These findings may explain why, in the present study, the degree of pancreatic inflammation and the pathological score of pancreatic tissue in the HTGP group were significantly greater than those in the AP group.

In this study, stimulation of HPDE6-C7 cells with CAE, a CCK analog, markedly elevated calcium ion levels in both the cytoplasm and mitochondria, accompanied by a significant upregulation of MCU expression. These findings were consistent with observations from the CAE-induced mouse AP model. Experimental results further demonstrated that treatment of HPDE6-C7 cells with CAE (10^{-7} mol/L) for 24 hours altered intracellular and mitochondrial calcium ion concentrations, as well as ROS and MCU levels. MCU expression in the AP and HTGP groups was significantly higher than in the control and TG groups; however, no notable difference was observed between the TG and control groups, or between the HTGP and AP groups. MCU primarily functions to mediate calcium ion transport from the cytoplasm into

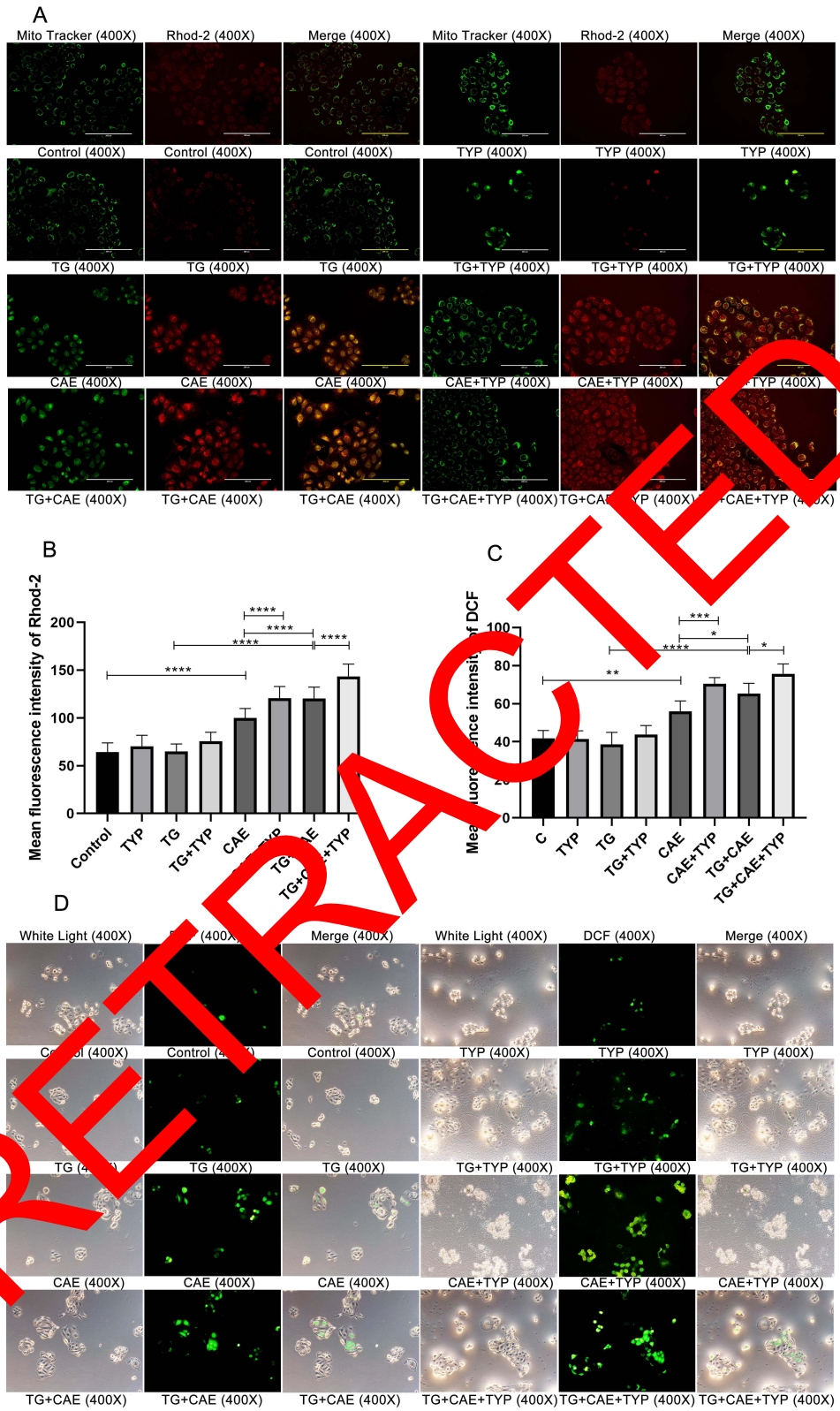

Figure 6 (**A**) Immunofluorescence images of the mitochondrial calcium ions in HPDE6-C7 cells in each group. The stronger the red fluorescence is, the higher the concentration of mitochondrial calcium ions. (**B**) The average fluorescence intensity of the mitochondrial calcium ions in HPDE6-C7 cells in each group. (**C**) The average fluorescence intensity of the ROS in HPDE6-C7 cells in each group. (**D**) Immunofluorescence images of the ROS in HPDE6-C7 cells in each group; the stronger the green fluorescence is, the higher the concentration of ROS; **P* < 0.05; ***P* < 0.01; ****P* < 0.001; *****P* < 0.0001.

Abbreviation: ROS, reactive oxygen species.

https://doi.org/10.2147/IJGM.S542782

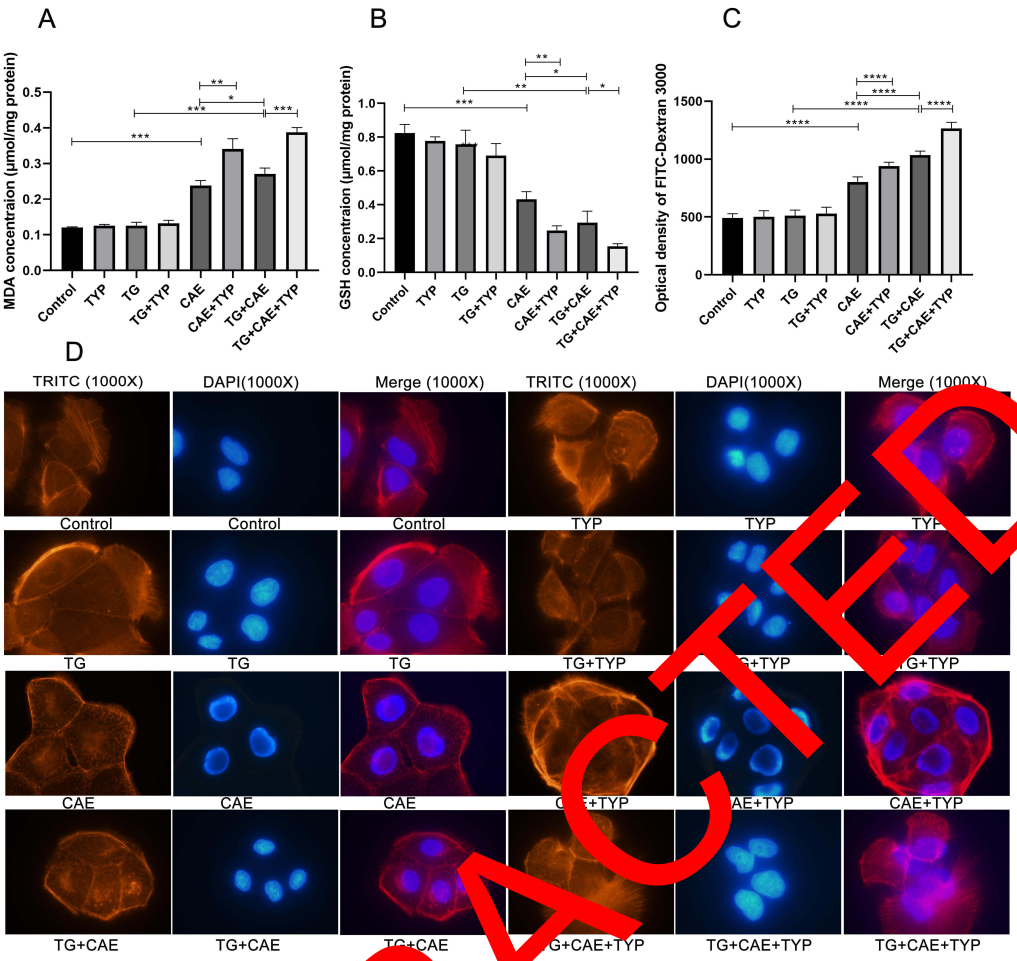

Figure 7 (**A**) Comparison of the MDA concentrations in HPDE6-C7 cells in each group. (**B**) Comparison of the GSH concentrations in HPDE6-C7 cells in each group. (**C**) Monolayer cell permeability of HPDE6-C7 cells in each group. (**D**) Microfilament cytoskeleton staining of HPDE6-C7 cells in each group, in which red indicates the microfilament cytoskeleton and blue indicates the nucleus. *P < 0.05; ***P < 0.001; ****P < 0.0001.

the mitochondria. Additionally, mitochondrial calcium concentrations in the HTGP and AP groups exceeded those in the TG and control groups, with a more substantial increase observed in the HTGP group compared to the AP group. In vitro analyses revealed that 24 h stimulation of HPDE6-C7 cells with CAE or TG+CAE significantly increased intracellular MCU expression, mitochondrial calcium ion levels, and ROS production, with the TG+CAE group exhibiting a greater elevation than the CAE group. Under physiological conditions, a certain level of calcium ions is required for mitochondrial oxidative phosphorylation and ATP synthesis.[37] We found that HPDE6C7 cells with low expression of MCU induced by lentivirus transfection presented abnormal growth, further verifying the importance of the MCU gene for HPDE6C7 cells under physiological conditions. However, under pathological conditions, the increase in calcium ion levels in mitochondria caused by high expression of MCU is the primary driver of ROS production in mitochondria. The excessive production of ROS can directly lead to metabolic disorders and cell death.[38] Interestingly, these changes in the mitochondrial calcium ion concentration and ROS can be reversed by treatment with ruthenium red, an active inhibitor of MCU. Therefore, we speculate that the MCU-induced increase in mitochondrial calcium levels may be an important factor leading to AP. The toxic effects of free fatty acids may also be involved, which may lead to an increase in intracellular calcium ions, mitochondrial calcium ions, and ROS,[39] which may explain the greater increase in intracellular calcium ions, mitochondrial calcium ions, and ROS in the TG+CAE group than in the CAE group.

The PDMB consists of a tightly packed pancreatic ductal epithelium and mucus that protects the pancreatic parenchyma from the contents of the pancreatic duct, such as bile and trypsin.[12] When PDMB is stimulated by inflammatory factors, septicemia, and chemicals, the cytoskeleton in pancreatic ductal epithelial cells is destroyed, and

the tight connections between cells are damaged, resulting in pancreatic tissue edema and destruction; these changes induce AP.[40] Actin filaments (AFs), also known as microfilaments (MFs), are among the main components of the cytoskeleton and play a key role in providing mechanical support and maintaining cell morphology. Damage to the MF cytoskeleton, which is involved in the regulation of intercellular connectivity through interactions with the cell membrane,[14] can ultimately damage the PDMB.[41] Our results revealed that the permeability of monolayer cells in the CAE and TG+CAE groups was significantly greater than that in the control and TG groups, and the degree of increase in the TG+CAE group was greater than that in the CAE group.

Additionally, the microfilament skeleton of HPDE6-C7 cells in the CAE and TG+CAE groups was significantly damaged, and the degree of damage to the microfilament skeleton was greater in the TG+CAE group. The MCU inhibitor ruthenium red reversed these changes. Therefore, we speculated that mitochondrial calcium overload and oxidative stress induced by an increase in MCU may be the causes of the destruction of the microfilament cytoskeleton and impairment of PDMB function. In an experimental study on Alzheimer's disease, the inhibition of MCU activity by ruthenium red improved mitochondrial calcium ion accumulation, mitochondrial function, and bioenergetics.[42] Similar results were also reported in a study on a disease model of subarachnoid hemorrhage.[43] Similarly, ruthenium red has a protective effect on cardiac ischemia and reperfusion injury (CIR) by reducing calcium accumulation in mitochondria.[44] Ruthenium red can also reduce the accumulation of calcium ions in the cytoplasm and mitochondria after traumatic brain injury.[45] These findings suggest that MCUs may be potential therapeutic targets for various diseases, including AP.

SIRT3 belongs to the Sirtuin family and protects mitochondria from damage.[24] SIRT3 modulates mitochondrial protein expression and activation, reduces ROS generation, and is important for mitochondrial adaptability and the stress response.[46] The expression of SIRT3 in the CAE group and TG+CAE group was significantly lower than that in the control group and TG group, and this change was reversed by RR intervention. After intervention with 3-TYP, the levels of active inhibitors of SIRT3, ROS, and MDA in the CAE group and TG+CAE group further increased, the levels of GSH and monolayer cell permeability further decreased, and the microfilament cytoskeleton was further damaged. Therefore, we speculated that MCU may be involved in the pathogenesis of AP by inhibiting the expression of SIRT3, resulting in increased oxidative stress and destruction of the microfilament cytoskeleton and PDMB functions.

However, this study had several limitations. First, the present study was based on animal and cellular data, which may be different from the real disease state in humans. Second, the specific mechanism by which MCUs increase oxidative stress and impair the function of PDMB need to be further investigated.

Conclusions

MCU may be involved in the pathogenesis of AP by inhibiting the expression of SIRT3, resulting in increased oxidative stress and destruction of the microfilament cytoskeleton and PDMB functions. The inhibition of MCU activity by RR can significantly reverse the above changes. Thus, MCU might be a potential target for treating AP.

Data Sharing Statement

Data will be made available on request from the corresponding author.

Acknowledgments

This work was supported by the Key Laboratory Project of Digestive Diseases in Jiangxi Province (2024SSY06101), and Jiangxi Clinical Research Center for Gastroenterology (20223BCG74011).

Author Contributions

All authors made a significant contribution to the work reported, whether that is in the conception, study design, execution, acquisition of data, analysis and interpretation, or in all these areas; took part in drafting, revising or critically reviewing the article; gave final approval of the version to be published; have agreed on the journal to which the article has been submitted; and agree to be accountable for all aspects of the work.

Funding

This work was supported by the National Natural Science Foundation of China [grant numbers 82460134]; Natural Science Foundation of Jiangxi Province [20232BAB206021].

Disclosure

The authors report no conflicts of interest in this work.

References

1. Yadav D, Lowenfels AB. Trends in the epidemiology of the first attack of acute pancreatitis: a systematic review. *Pancreas*. 2006;33(4):323–330. doi:10.1097/01.mpa.0000236733.31617.52
2. Schepers NJ, Bakker OJ, Besselink MG, et al. Impact of characteristics of organ failure and infected necrosis on mortality in necrotising pancreatitis. *Gut*. 2019;68(6):1044–1051. doi:10.1136/gutjnl-2017-314657
3. Gurusamy KS, Belgaumkar AP, Haswell A, Pereira SP, Davidson BR. Interventions for necrotising pancreatitis. *Cochrane Database Syst Rev*. 2016;4(4):CD011383. doi:10.1002/14651858.CD011383.pub2
4. Bang JY, Wilcox CM, Arnoletti JP, Varadarajulu S. Superiority of endoscopic interventions over minimally invasive surgery for infected necrotizing pancreatitis: meta-analysis of randomized trials. *Dig Endosc*. 2020;32(3):298–308. doi:10.1111/den.13[illegible]0
5. Pirillo A, Casula M, Olmastroni E, Norata GD, Catapano AL. Global epidemiology of dyslipidaemias. *Nat Rev Cardiol*. 2021;18(10):689–700. doi:10.1038/s41569-021-00541-4
6. Krishna SG, Kamboj AK, Hart PA, Hinton A, Conwell DL. The changing epidemiology of acute pancreatitis hospitalizations: a decade of trends and the impact of chronic pancreatitis. *Pancreas*. 2017;46(4):482–488. doi:10.1097/MPA.0000000000000783
7. Párniczky A, Kui B, Szentesi A, et al. Prospective, multicentre, nationwide clinical data from 600 cases of acute pancreatitis. *PLoS One*. 2016;11(10):e0165309. doi:10.1371/journal.pone.0165309
8. Dancu G, Bende F, Danila M, Sirli R, Popescu A, Tarta C. Hypertriglyceridemia-induced acute pancreatitis: a different disease phenotype. *Diagnostics*. 2022;12(4):868. doi:10.3390/diagnostics12040868
9. De Pretis N, De Marchi G, Frulloni L. Hypertriglyceridemic pancreatitis. *Minerva Gastroenterologica e Dietologica*. 2020;66(3):238–245. doi:10.23736/S1121-421X.19.02641-2
10. Guo YY, Li HX, Zhang Y, He WH. Hypertriglyceridemia-induced acute pancreatitis: progress on disease mechanisms and treatment modalities. *Discov Med*. 2019;27(147):101–109.
11. Valdivielso P, Ramírez-Bueno A, Ewald N. Current knowledge of hypertriglyceridemic pancreatitis. *Eur J Intern Med*. 2014;25(8):689–694. doi:10.1016/j.ejim.2014.08.008
12. Konok GP, Thompson AG. Pancreatic ductal mucosa as a protective barrier in the pathogenesis of pancreatitis. *Am J Surg*. 1969;117(1):18–23. doi:10.1016/0002-9610(69)90280-3
13. Svitkina TM. Ultrastructure of the actin cytoskeleton. *Curr Opin Cell Biol*. 2018;54:1–8. doi:10.1016/j.ceb.2018.02.007
14. Sakakibara S, Maruo T, Miyata M, Mizutani K, [illegible]kai Y. [illegible]nt of the F-actin-binding activity of l-afadin for enhancing the formation of adherens and tight junctions. *Genes Cells*. 2018;23([illegible])[illegible]–199. doi:10.1111/gtc.12566
15. Shakhov AS, Dugina VB, Alieva IB. Structural features of actin cytoskeleton required for endotheliocyte barrier function. *Biochem Biokhimiia*. 2019;84(4):358–369. doi:10.1134/S0006297919040035
16. Izadi M, Hou W, Qualmann B, Kessels MM. Direct effects of Ca(2+)/calmodulin on actin filament formation. *Biochem Biophys Res Commun*. 2018;506(2):355–360. doi:10.1016/j.bbrc.2018.[illegible]159
17. Wei B, Gong Y, Yang H, Zhang J, Su Z, Liang Z. Role of tumor necrosis factor receptor-associated factor 6 in pyroptosis during acute pancreatitis. *Mol Med Rep*. 2021;24([illegible]doi:10.3892/mmr.2021.12488
18. De Stefani D, Raffaello A, Teardo E, Szabò I, Rizzuto R. A forty-kilodalton protein of the inner membrane is the mitochondrial calcium uniporter. *Nature*. 2011;476(7360):33[illegible]. doi:10.1038/nature10230
19. Zhao H, Chen S[illegible] et al. Berberine as a novel mitochondrial calcium uniporter inhibitor that disrupts MCU-EMRE assembly. *Adv Sci*. 2025;12(17):e241231[illegible]doi:10.1002/advs.[illegible]2311
20. Angelova PR, Abramov AY. Interplay of mitochondrial calcium signalling and reactive oxygen species production in the brain. *Biochem Soc Trans*. 2024;52(4):[illegible]39–10[illegible]. doi:[illegible]42/BST20240261
21. Yu X, Dai C, [illegible]o X, et al. Ruthenium red attenuates acute pancreatitis by inhibiting MCU and improving mitochondrial function. *Biochem Biophys Res Commun*. 2022;635:236–243. doi:10.1016/j.bbrc.2022.10.044
22. Oppedisano F, Nesci S, Spagnoletta A. Mitochondrial sirtuin 3 and role of natural compounds: the effect of post-translational modifications on cellular metabolism. *Crit Rev Biochem Mol Biol*. 2024;59(3–4):199–220. doi:10.1080/10409238.2024.2377094
23. Meng N, Yang H, Chen J, et al. Honokiol reduces oxidative stress by activating the SIRT3-MnSOD2 pathway to alleviate hypertriglyceridemia-induced acute pancreatitis in rats. *Nan Fang Yi Ke Da Xue Xue Bao*. 2023;43(3):405–411. doi:10.12122/j.issn.1673-4254.2023.03.10
24. Jin H, Zhao K, Li J, Xu Z, Liao S, Sun S. Matrine alleviates oxidative stress and ferroptosis in severe acute pancreatitis-induced acute lung injury by activating the UCP2/SIRT3/PGC1α pathway. *Int Immunopharmacol*. 2023;117:109981. doi:10.1016/j.intimp.2023.109981
25. Van Laethem JL, Marchant A, Delvaux A, et al. Interleukin 10 prevents necrosis in murine experimental acute pancreatitis. *Gastroenterology*. 1995;108(6):1917–1922. doi:10.1016/0016-5085(95)90158-2
26. Lerch MM, Gorelick FS. Models of acute and chronic pancreatitis. *Gastroenterology*. 2013;144(6):1180–1193. doi:10.1053/j.gastro.2012.12.043
27. Sun W, Chen Y, Li H, et al. Material basis and molecular mechanisms of Dachengqi decoction in the treatment of acute pancreatitis based on network pharmacology. *Biomed Pharmacother*. 2020;121:109656. doi:10.1016/j.biopha.2019.109656

28. Fu X, Li P, Yin W, et al. Overexpression of Nrf2 protects against lipopolysaccharide and cerulein-induced pancreatitis in vitro and in vivo. *Pancreas*. 2020;49(3):420–428. doi:10.1097/MPA.0000000000001501
29. Xue BH, Liu Y, Chen H, Sun Y, Yu WL. A novel function of IRF9 in acute pancreatitis by modulating cell apoptosis, proliferation, migration, and suppressing SIRT1-p53. *Mol Cell Biochem*. 2020;472(1–2):125–134. doi:10.1007/s11010-020-03791-x
30. Yang H, Liang Z, Xie J, et al. Gelsolin inhibits autophagy by regulating actin depolymerization in pancreatic ductal epithelial cells in acute pancreatitis. *Braz J Med Biol Res*. 2023;56:e12279. doi:10.1590/1414-431x2023e12279
31. Yang HY, Liang ZH, Xie JL, et al. Gelsolin impairs barrier function in pancreatic ductal epithelial cells by actin filament depolymerization in hypertriglyceridemia-induced pancreatitis in vitro. *Exp Ther Med*. 2022;23(4):290. doi:10.3892/etm.2022.11219
32. Yang AL, McNabb-Baltar J. Hypertriglyceridemia and acute pancreatitis. *Pancreatology*. 2020;20(5):795–800. doi:10.1016/j.pan.2020.06.005
33. Noel P, Patel K, Durgampudi C, et al. Peripancreatic fat necrosis worsens acute pancreatitis independent of pancreatic necrosis via unsaturated fatty acids increased in human pancreatic necrosis collections. *Gut*. 2016;65(1):100–111. doi:10.1136/gutjnl-2014-308043
34. Khatua B, Yaron JR, El-Kurdi B, Kostenko S, Papachristou GI, Singh VP. Ringer's lactate prevents early organ failure by providing extracellular calcium. *J Clin Med*. 2020;9(1):263. doi:10.3390/jcm9010263
35. Dambrauskas Z, Giese N, Gulbinas A, et al. Different profiles of cytokine expression during mild and severe acute pancreatitis. *World J Gastroenterol*. 2010;16(15):1845–1853. doi:10.3748/wjg.v16.i15.1845
36. Aoun E, Chen J, Reighard D, Gleeson FC, Whitcomb DC, Papachristou GI. Diagnostic accuracy of interleukin-6 and interleukin-8 in predicting severe acute pancreatitis: a meta-analysis. *Pancreatology*. 2009;9(6):777–785. doi:10.1159/000214191
37. Peng TI, Jou MJ. Oxidative stress caused by mitochondrial calcium overload. *Ann N Y Acad Sci*. 2010;1201(1):183–188. doi:10.1111/j.1749-6632.2010.05634.x
38. Wang Y, Li X, Zhao F. MCU-Dependent mROS generation regulates cell metabolism and cell death modulated by the AMPK/PGC-1α/SIRT3 signaling pathway. *Front Med*. 2021;8:674986. doi:10.3389/fmed.2021.674986
39. Criddle DN, Raraty MG, Neoptolemos JP, Tepikin AV, Petersen OH, Sutton R. Ethanol toxicity in pancreatic acinar cells: mediation by nonoxidative fatty acid metabolites. *Proc Natl Acad Sci U S A*. 2004;101(29):10738–10743. doi:10.1073/pnas.0402911101
40. Quilichini E, Fabre M, Dirami T, et al. Pancreatic ductal deletion of Hnf1b disrupts exocrine homeostasis, leading to pancreatitis, and facilitates tumorigenesis. *Cell Mol Gastroenterol Hepatol*. 2019;8(3):487–511. doi:10.1016/j.jcmgh.2019.06.005
41. Wang J, Qin M, Wu Q, et al. Effects of lipolysis-stimulated lipoprotein receptor on tight junctions of pancreatic ductal epithelial cells in hypertriglyceridemic acute pancreatitis. *Biomed Res Int*. 2022;2022(1):4234186. doi:10.1155/2022/4234186
42. Sharma Y, Garabadu D. Ruthenium red, mitochondrial calcium uniporter inhibitor, attenuates cognitive deficits in STZ-ICV challenged experimental animals. *Brain Res Bull*. 2020;164:121–135. doi:10.1016/j.brainresbull.2020.08.020
43. Yan H, Hao S, Sun X, et al. Blockage of mitochondrial calcium uniporter prevents iron accumulation in a model of experimental subarachnoid hemorrhage. *Biochem Biophys Res Commun*. 2015;456(4):835–840. doi:10.1016/j.bbrc.2014.12.073
44. Menezes-Rodrigues FS, Tavares JGP, Vasques ER, et al. Cardioprotective effects of pharmacological blockade of the mitochondrial calcium uniporter on myocardial ischemia-reperfusion injury. *Acta Cir Bras*. 2020;35(5):e202000306. doi:10.1590/s0102-865020200030000006
45. Zhang L, Wang H, Zhou X, Mao L, Ding K, Hu Z. Role of mitochondrial calcium uniporter-mediated Ca(2+) and iron accumulation in traumatic brain injury. *J Cell Mol Med*. 2019;23(4):2995–3009. doi:10.1111/jcmm.14202
46. Hallows WC, Albaugh BN, Denu JM. Where in the cell is SIRT3—functional localization of an NAD+-dependent protein deacetylase. *Biochem J*. 2008;411(2):e11–e13. doi:10.1042/BJ20080336